Available online at www.sciencedirect.com
SCIENCE DIRECT®
Catalysis Today 105 (2005) 647–654
CATALYSIS TODAY
www.elsevier.com/locate/cattod

Marvelous self-assembly of hierarchically nanostructured porous zirconium phosphate solid acids with high thermal stability

Zhong-Yong Yuan [a,*], Tie-Zhen Ren [a], Ammar Azioune [b], Jean-Jacques Pireaux [b], Bao-Lian Su [a,*]

[a] *Laboratoire de Chimie des Matériaux Inorganiques (CMI), The University of Namur (FUNDP), 61 rue de Bruxelles, B-5000 Namur, Belgium*
[b] *Laboratoire Interdisciplinaire de Spectroscopie Electronique (LISE), The University of Namur (FUNDP), 61 rue de Bruxelles, B-5000 Namur, Belgium*

Available online 11 July 2005

Abstract

A hierarchical structure of thermally stable macroporous zirconium phosphate solid acids with supermicroporous walls was prepared by a simple self-assembly process from the precursors of zirconium propoxide and orthophosphoric acid solution. The macroporous structures are uniform with the diameters ranging from 300 to 800 nm, one-dimensional channel-like. The effect of surfactant Brij 56 on the formation of macroporous structures has been studied. The frameworks of the synthesized hierarchical zirconium phosphates are amorphous with Zr–O–P bonding, exhibiting remarkably high thermal stability (at least 800 °C), on the basis of the X-ray diffraction (XRD), N_2 adsorption, X-ray photoelectron spectroscopy (XPS) analysis, Fourier transform infrared (FT-IR) and ^{31}P nuclear magnetic resonance (NMR) spectra. Larger quantities of Zr–OH and P–OH groups are observed besides surface hydroxyl groups, suggesting the presence of acidity and the possibility of surface functionalization for practical applications including catalysis. The macroporous zirconium phosphates with hierarchical structures could also be the potential and efficient catalyst supports for the design of the structured catalysts and reactors.

Keywords: Macroporous structure; Supermicroporosity; Zirconium phosphate; Self-assembly; Acidic property

1. Introduction

Porous and high-surface-area materials are of great interest to many scientific communities [1]. Nanoporous materials with hierarchical structures have recently attracted significant attention because they combine the advantages of high surface area with the accessible diffusion pathways associated with macroporous structures. Bimodal mesoporous–macroporous oxide materials may be obtained by dual templating, i.e. the combination of the surfactant [2] or block copolymer [3] templating techniques and the micromould methods of emulsion/vesicle droplets [4,5] or colloid crystals [6,7], or bacterial threads [8]. By utilization of zeolitic nanoparticles in combination with latex spheres, micro-macroporous materials have been synthesized [9,10]. Hierarchical trimodal porous silica was synthesized by using poly(styrene) spheres, a block copolymer, and an ionic liquid as templates [11], exhibiting a well-defined macropore structure and bimodal mesoporosity. Chemical means of inducing phase and domain separation during synthesis have also been applied in the production of siliceous materials having a hierarchical porosity [12,13], but the resultant macroporous structures were nonuniform. The construction of both mesoporous and macroporous structures in one body has recently been demonstrated to be accessible in the presence of one single surfactant [14–18], without the need of secondary templates such as colloid crystals and emulsions, and the ordered macropores were mainly one-dimensional channel-like, distinct from those templated by emulsion droplets or colloid crystals.

Zirconium phosphate is one of the most studied members of the well-known family of layered solid acids [19]. Surfactant-assisted methods have been used to prepare porous

* Corresponding authors. Tel.: +32 81 4531; fax: +32 81 725414.
E-mail addresses: zhong-yong.yuan@fundp.ac.be (Z.-Y. Yuan), bao-lian.su@fundp.ac.be (B.-L. Su).

0920-5861/$ – see front matter © 2005 Elsevier B.V. All rights reserved.
doi:10.1016/j.cattod.2005.06.038

zirconium phosphates of mesophases for potential application as catalysts and catalyst supports [20,21], in which phosphoric acid was directly used at the stage of the formation of inorganic matrix. However, highly ordered structural phases were not observed in these surfactant-synthesized mesoporous zirconium phosphates. A phosphoric acid treatment of a mesostructured zirconium sulfate surfactant composite could lead to high-surface-area zirconium oxophosphate [22]. Although highly ordered, stable mesoporous metal phosphates have been synthesized by Zhao and co-workers recently based on an ''acid–base pair'' route by using triblock copolymer as a template [23], little concerns on the synthesis of hierarchical porous zirconium phosphate materials with multiple-scaled porosity to date [24]. We present herein a marvelous self-assembly of hierarchically porous nanostructured zirconium phosphate solid acids with uniform macroporous system. Neither colloid crystals nor emulsion droplets were needed for the creation of uniform macropores, and the hierarchical structure of zirconium phosphate was spontaneously formed, possessing a uniform macroporous system with nanoporous walls, which should be significant from a technological point of view. Such a hierarchical porous structure enables our synthesized zirconium phosphates to efficiently reduce diffusion resistance of molecules for yielding improved overall reaction, which are really desirable catalysts or catalyst supports for the design of structured catalysts, or one-pot reactors. Here, we just report the first step of our general work on the rational design of hierarchically porous materials and their applications in catalysis and other fields.

2. Experimental

2.1. Synthesis of materials

All chemicals were used as received without further purification. In a typical synthesis procedure, 0.01 mol of zirconium *n*-propoxide ($Zr(OC_3H_7)_4$, 70 wt% solution in 1-propanol, Aldrich) was added into a pre-treated 60 mL solution of orthophosphoric acid (0.1 mol/L) in the presence or absence of 6.67 g (0.01 mol) surfactant Brij 56 ($C_{16}(EO)_{10}$, Aldrich) under stirring. After a further stirring of 2 h at room temperature, the obtained mixture was separated into two parts: one was transferred into a Teflon-lined autoclave and aged statically at 80 °C for 24 h (denoted as ZrP-h), and another was directly filtered, washed with water, and dried at 60 °C (denoted as ZrP-d) for comparing. The obtained white ZrP-h solid was then calcined at 500, 650 or 800 °C for 1 h, denoted as ZrP-hc500, ZrP-hc650 and ZrP-hc800, respectively, and the ZrP-d was calcined at 500 °C, denoted as ZrP-dc500, to investigate the thermal stability.

2.2. Characterization

Powder X-ray diffraction (XRD) patterns were recorded on a Philips PW1820 diffractometer with Cu Kα radiation. N_2 adsorption and desorption isotherms were obtained on a Micromeritics Tristar 3000 system at liquid nitrogen temperature. The samples were degassed at 80 °C overnight before measurements were made. The specific surface area was determined by the Brunauer–Emmett–Teller (BET) method and the pore size distribution was obtained from the N_2 adsorption branch of isotherms using the Barrett–Joyner–Halenda (BJH) method. Although it is well-known that the BJH method gives underestimated pore size values and some new interesting methods have been developed recently by Kruk and Jaroniec [25], we used the BJH method here for the sake of simplicity, and this mathematical algorithm would not affect significantly our systematic comparison.

Scanning electron microscopy (SEM) and transmission electron microscopy (TEM) were carried out with Philips XL-20 at 15 keV and Philips TECNAI-10 at 100 kV, respectively. The specimens for TEM observation were prepared by epoxy resin imbedded micro-sectioning and mounting on a copper grid.

Solid-state ^{31}P magic angle spinning (MAS) nuclear magnetic resonance (NMR) spectra were recorded on a Bruker MSL-400 spectrometer operating at resonance frequencies of 161.9 MHz, and 2.5 μs ($\theta = \pi/6$) pulse with repetition time of 10 s. Chemical shifts were indicated using an external 85% H_3PO_4 reference.

Fourier transform infrared (FT-IR) spectroscopy was performed with a Perkin-Elmer Spectrum 2000 spectrometer. KBr pellet technique was used for the framework vibration characterization. For the study of the surface acidity, a self-supported wafer of zirconium phosphate sample was in situ evacuated at 450 °C for 3 h, followed by adsorption of NH_3 at room temperature for 15 min, and desorption at different temperatures (100–300 °C) for 15 min, respectively.

X-ray photoelectron spectroscopy (XPS) measurements were realized on a Hewlett-Packard 5950A spectrometer equipped with a monochromatic Al Kα source (1486.6 eV). Charging effects were neutralized using a flood gun typically operated at 2 eV. The take-off angle analysis relative to the surface was 52°. All the spectra showed a small shift due to charging and were therefore calibrated in relation to the C 1s peak of contamination (285.0 eV). The photoemission peaks were fitted with mixed Gaussian–Lorentzian functions using a home-developed (LISE) least squares curve-fitting program (Winspec). Both linear and Shirley backgrounds were used depending on the shape of spectra. The surface atomic composition was calculated by the integration of the peak areas on the basis of the Scofield's sensitivity factors.

3. Results and discussion

3.1. Porous hierarchy visualized by electron microscopy

The hierarchically porous zirconium phosphate materials were prepared by the direct reaction of zirconium propoxide

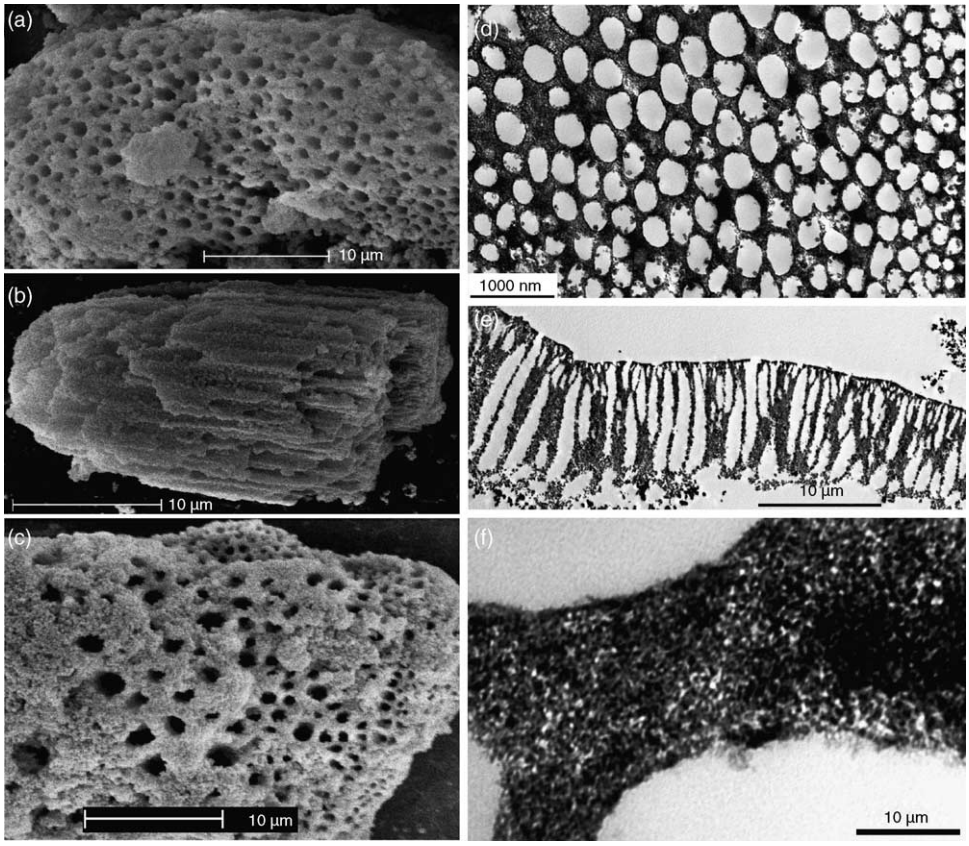

Fig. 1. SEM images of: (a and b) the hierarchical ZrP-h sample synthesized in the absence of surfactant and (c) its 650 °C-calcined product ZrP-hc650; (d and e) low-magnification and (f) high-magnification cross-sectional TEM images of (a and b).

and phosphoric acid in the absence or presence of nonionic surfactant Brij 56. Fig. 1 shows the typical SEM and cross-sectional TEM images of the surfactantless-synthesized ZrP-h samples. It is clearly revealed from the SEM images (Fig. 1a) that these surfactantless-synthesized samples have a uniform macroporous structure, distributed in the whole particles of several micrometers to several tens micrometers in sizes. The macropores are of regular array with the diameters ranging from 300 to 800 nm. The hollow macrochannels are practically parallel to each other, and extend throughout almost the whole particles (Fig. 1b). The regularity of macropores is further confirmed by the cross-sectional TEM images (Fig. 1d and e). The high-magnification TEM images also reveal that the macroporous framework is mesostructured with a disordered wormhole-like assembly of accessible meso/micropores (Fig. 1f). It is substantially significant that such a hierarchically macroporous structure is thermally stable. Fig. 1c is the SEM image of the sample after calcination at 650 °C, showing very good macroporous structure, in spite of the local damage of the macrochannels.

The similar macroporous structures can be also seen in the ZrP-h sample prepared with surfactant (Fig. 2), as well as in the ZrP-d samples obtained in the presence/absence of surfactant but without autoclaving; however, the quantities of the macrochannel of last samples are relatively low with poor macroporosities. This indicates that the self-formation of macroporous structures was initiated before autoclaving of the reaction system. And it seems that the addition of surfactant did not induce a positive effect on the formation of the macroporous structures while hierarchically meso-macroporous pure zirconia previously reported, where high yield of well-defined macroporous structure was obtained in the presence of either nonionic or cationic surfactant [14,17]. Since the pH values of the reaction systems of this work are almost the same with those of pure hierarchical zirconias (pH $\approx$ 2), phosphatic species may affect the macrochannels formation when in the presence of surfactant.

The formation of the macroporous structures with nanostructured walls is spontaneous, since no templates or structure-directing agents are necessary. The hydrolysis of Zr-alkoxide precursors in the phosphate solution would result in the rapid formation of nanometer-sized zirconium phosphate particles. A lot of propanol molecules were quickly and simultaneously generated by the reaction of zirconium propoxide and phosphatic ions and the poly-condensation, which might produce microphase-separated domains of zirconium phosphate-based nanoparticles and water/alcohol channels that are the initiators of the macrochannels [24]. Autoclaving would consolidate the regular self-assembly of the nanoparticles, creating a well-connected network of mesoporous/microporous walls

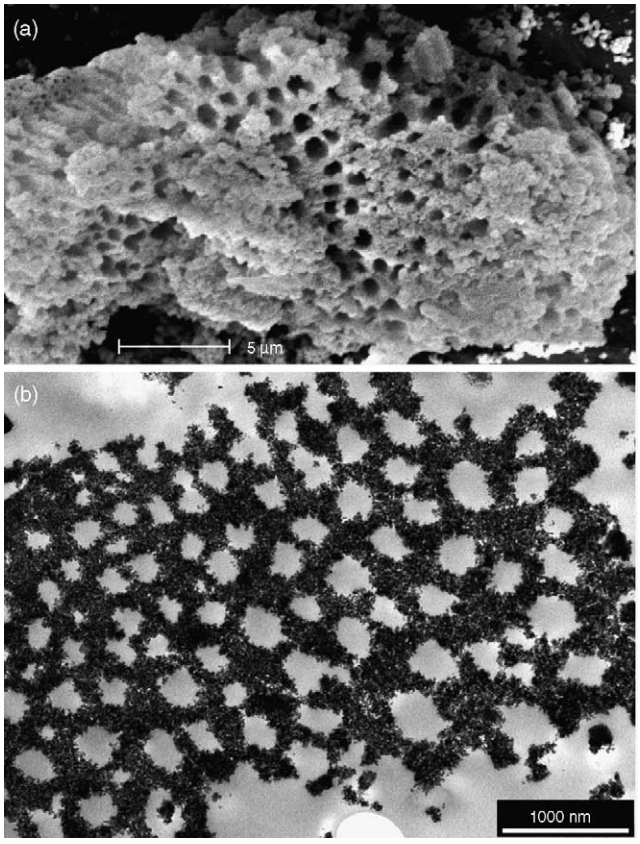

Fig. 2. (a) SEM and (b) cross-sectional TEM images of the ZrP-h sample synthesized in the presence of surfactant.

between macrochannels. Thus, a hierarchical nanoporous structure of nanoparticle assembly would form during the synergistic packing of the nanoparticles and rapid release of propanol molecules. The surfactant molecules may affect the precipitation and polycondensation of the zirconium phosphate nanoparticles, leading to the relative poor quantity of the resultant macroporous structure.

3.2. Porosities and nature of the framework by N_2 adsorption and X-ray diffraction

The nanostructures of the macroporous zirconium phosphate walls, observed by the TEM images, were also confirmed by the N_2 adsorption analysis. Fig. 3 shows the N_2 adsorption–desorption isotherms of the surfactantless-synthesized ZrP-h sample and its calcined products and their corresponding pore size distribution curves. All samples before and after calcination exhibit the isotherms between types IV and II. The adsorption isotherms exhibit a high uptake of N_2 at low relative pressure (P/P_0) of 0.1–0.40, indicating the presence of pores with the pore size ranging 1–2 nm (between micropore and mesopore sizes). The analysis of the pore size distribution by the BJH method from the adsorption branch of the isotherms reveals a narrow pore size distribution centered at 1.7 nm for the surfactant-less-synthesized ZrP-h sample, and the pore sizes of 1.4–

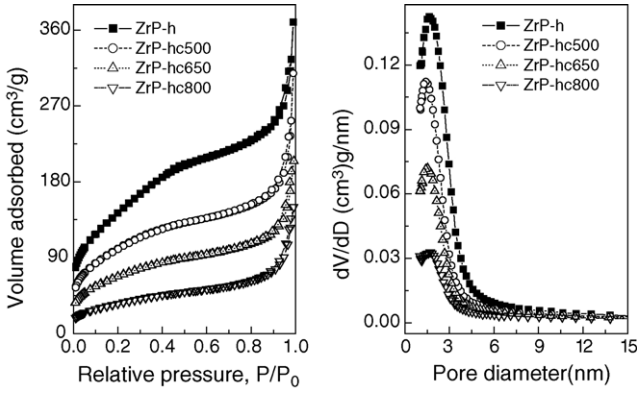

Fig. 3. N_2 adsorption–desorption isotherms (left) and the corresponding pore size distribution curves (right) of the hierarchical zirconium phosphate samples synthesized in the absence of surfactant.

1.7 nm for the calcined samples (Table 1). This trend is in accord with the pore size distributions calculated from the desorption branches. The pores with the sizes in this range can be regarded as ''supermicropores''. Meanwhile, at the relative pressure higher than 0.85, a strong increase in nitrogen adsorbed volume is observed, evident of an appreciable amount of secondary porosity, i.e. the very large mesopores or macropores. This secondary porosity should be related to the macropores revealed by SEM and TEM images. The secondary porosity, as well as the uniform supermicroporosity, can be clearly seen in the samples calcined even at 800 °C, indicative of the high thermal stability. A very high specific surface area of 528 m^2/g is obtained with pore volume of 0.57 cm^3/g for the surfactant-less-synthesized ZrP-h, which is comparable to the previously reported surfactant-templated meso-macroporous ZrO_2 [17], and practically higher than that of the triblock copolymer-templated mesoporous zirconium phosphate [23]. Although the surface areas and pore volumes decrease with the increase of the calcination temperature (Table 1), a high surface area of 132 m^2/g with a pore volume of 0.23 cm^3/g and a narrow pore size distribution centered at 1.7 nm can still be obtained after calcination at 800 °C.

The isotherms of the surfactant-synthesized ZrP-h are different (Fig. 4). Only very little adsorption was observed, which may be due to the surfactant molecules in the pore channels of the sample. Since the ZrP-d sample synthesized with surfactant but without autoclaving exhibits a comparatively high surface area of 228 m^2/g with a pore volume of 0.24 cm^3/g, it seems that the surfactant molecules blocked the pore opens during autoclaving. After calcination to remove the surfactant species, the samples present high surface areas (Table 1), though lower than the calcined samples obtained without surfactant. And the pore sizes of the surfactant-synthesized samples are also slightly smaller than those of the surfactantless-synthesized samples. This result means that the surfactant did not conduct to the improvement of the surface areas and porosities during the formation of zirconium phosphates, which is contrary to the

Table 1
Textural properties of the as-prepared hierarchical porous zirconium phosphate materials and their calcined products at different temperatures

Sample	S_{BET} (m^2/g)	V_{pore} (cm^3/g)	$D_{BJH\text{-}ads}$ (nm)	$D_{BJH\text{-}des}$ (nm)	S_{micro} (m^2/g)	V_{micro} (cm^3/g)
Synthesized without surfactant						
ZrP-h	528	0.572	1.65	1.77	24	0.001
ZrP-hc500	369	0.478	1.41	1.27	72	0.025
ZrP-hc650	248	0.317	1.53	1.52	43	0.014
ZrP-hc800	132	0.232	1.71	1.58	8	0.001
ZrP-d	200	0.251	–	–	106	0.048
ZrP-dc500	72	0.254	–	–	16	0.006
Synthesized with surfactant						
ZrP-h	10	0.090	–	–	–	–
ZrP-hc500	283	0.312	1.32	1.24	100	0.040
ZrP-hc650	234	0.272	1.32	1.21	85	0.034
ZrP-hc800	95	0.149	1.48	1.47	18	0.006
ZrP-d	228	0.235	–	–	125	0.055
ZrP-dc500	113	0.239	–	–	49	0.021

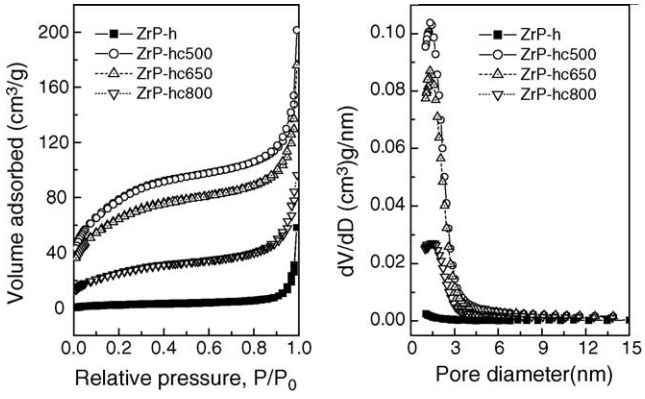

Fig. 4. N_2 adsorption–desorption isotherms (left) and the corresponding pore size distribution curves (right) of the hierarchical zirconium phosphate samples synthesized in the presence of surfactant.

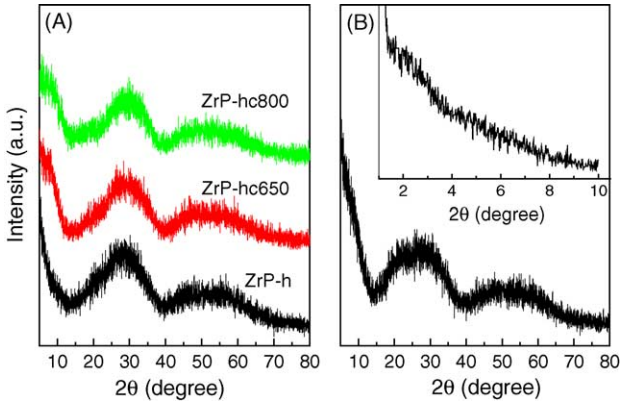

Fig. 5. (A) XRD patterns of surfactantless-synthesized ZrP-h and its calcined products ZrP-hc650 and ZrP-hc800 and (B) wide-angle and low-angle (inset) XRD patterns of the surfactant-synthesized ZrP-h.

case of pure zirconia [26]. The *t*-plot analysis also revealed a significant quantity of microporosity in the calcined zirconium phosphates synthesized with surfactant (Table 1), which is larger than the surfactantless-synthesized samples.

Powder X-ray diffraction patterns of the as-synthesized and calcined zirconium phosphate samples exhibit only two very broad peaks in the 2θ range of 15–35° and 40–70°, indicative of the amorphous nature of the framework walls (Fig. 5). No crystallized $ZrPO_4$ and/or ZrO_2 phases appear even after calcination at 800 °C. No narrow low-angle diffraction peaks were observed in the 2θ range from 1.0° to 3.0° for the samples synthesized either with or without surfactant, indicating that there is no long-range order of meso/micropore array in these hierarchical zirconium phosphate materials, since such narrow low-angle diffractions are characteristic of ordered mesoporous materials [2,3].

3.3. Chemical composition and atomic environment by XPS and NMR spectroscopy

The surface stoichiometry characterization was performed by XPS. Fig. 6 shows the high-resolution XPS spectra of Zr, P and O taken on the surface of the surfactantless-synthesized ZrP-h, which is taken as representative. The Zr 3d line is composed of two single peaks situated at 183.1 eV for the Zr $3d_{5/2}$ and 185.7 eV for the Zr $3d_{3/2}$. These binding energies are characteristic of Zr^{4+} [27]. The P 2p binding energy is observed at 133.8 eV, which is characteristic of P^{5+} [28]. The O 1s line might be fitted by three components situated at the binding energies of 530.6, 531.8 and 533.5 eV, which may correspond to oxygen combined with zirconium, phosphorus and carbon, respectively [29,30]. The O 1s component of the O–P bonds is dominant. The surface atomic compositions of the synthesized zirconium phosphate samples are summarized in Table 2. Very little change was seen in the surface atomic compositions of the surfactantless-synthesized samples before and after calcination, in which the measured carbon component and the excess oxygen are from the surface-absorbed organic contaminant and the surface-absorbed water, respectively. High content of carbon was observed in the surfactant-synthesized ZrP-h, indicating the occupied/adsorbed surfactant molecules, which also lead to the overhigh O/P and O/Zr ratios. Slight increase of Zr/P ratio

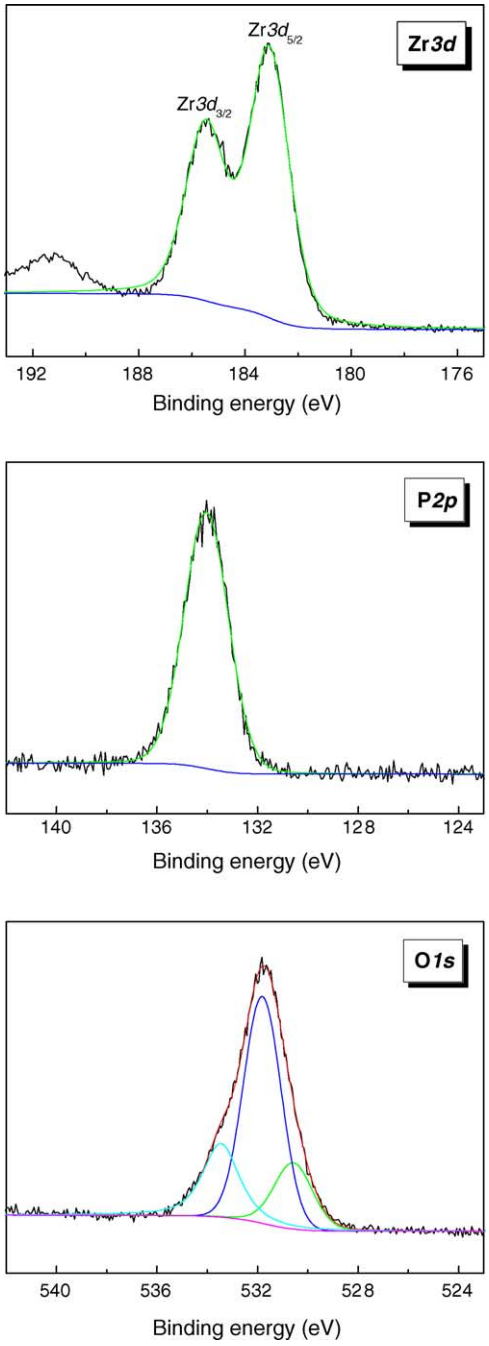

Fig. 6. High-resolution XPS spectra of the Zr 3d, P 2p and O 1s regions taken on the surface of the surfactantless-synthesized ZrP-h sample.

was seen after calcination, though the Zr/P ratios are still near 1, whatever the samples were synthesized with or without surfactant. The Zr/P ratios confirm the exclusive formation of zirconium polyphosphates.

^{31}P magic angle spinning NMR spectroscopy has been employed to study the phosphorus micro-environments. Both the as-prepared and calcined zirconium phosphates show the peaks between −13 and −19 ppm (Fig. 7), which could be attributed to tetrahedral phosphorus atoms bonded to three ZrO_4 units [20,31,32], i.e. [$(P(OZr)_3OH$]. Calcination

Table 2
The surface atomic compositions of the hierarchical zirconium phosphate materials, determined by XPS

Sample	Composition[a] (%)				O/Zr ratio	Zr/P ratio	O/P ratio
	O	Zr	P	C			
ZrP-h[b]	40	7.4	9.6	43	5.4	0.8	4.1
ZrP-hc650[b]	40.4	7.6	9	43	5.3	0.9	4.5
ZrP-h[c]	20.7	1.4	1.4	76.4	14.7	1	14.5
ZrP-hc650[c]	34.1	6.3	5.3	54.3	5.4	1.2	6.4

[a] Based on XPS line areas of O 1s, Zr 3d, P 2p and C 1s.
[b] Synthesized without surfactant.
[c] Synthesized with surfactant.

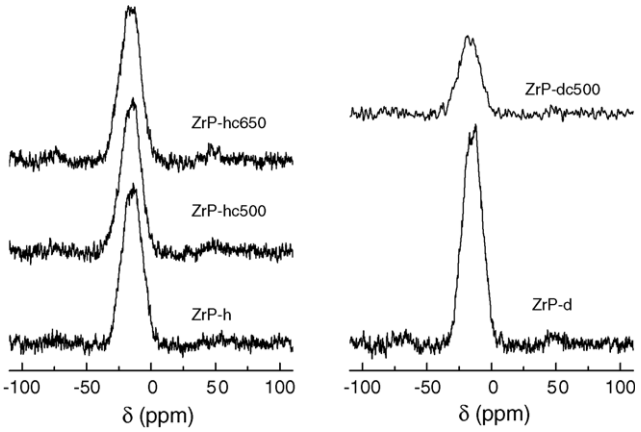

Fig. 7. ^{31}P MAS NMR spectra of the as-synthesized and calcined zirconium phosphate materials synthesized in the absence of surfactant.

did not result in the shift of the ^{31}P NMR signals, suggestive of the stable coordination environment of phosphorus. The relatively broad resonance may be due to the amorphous nature of the frameworks, lacking the atomic resolution that presented in the crystalline microporous phosphates.

3.4. Surface acidity by FT-IR spectroscopy

The FT-IR spectra of framework vibration of ZrP-h and ZrP-hc650 samples synthesized with or without surfactant are shown in Fig. 8. The spectrum of the surfactant-synthesized ZrP-h sample exhibits absorption bands in the region of 2850–2920 cm^{-1}, attributed to the C–H stretching mode of hydrocarbons, and the band at 1460 cm^{-1}, assigned to the bending vibration of the C–H band of methylene groups of the surfactant alkyl chain, which disappear after calcination. These C–H bands are not observed in the surfactantless-synthesized samples. The broad band around 3400 cm^{-1} and the band at 1630 cm^{-1} correspond to the surface-adsorbed water and hydroxyl groups [33]. The absence of phosphoryl (P=O) peaks at 1300–1400 cm^{-1} suggests the absence of PO_4^{3-} in the samples. And also, no distinct bands around 750 cm^{-1}, corresponding to P–O–P deformation vibrations [20], are observed in the IR spectra of all samples. Thus, it is indicated that the phosphorus exists

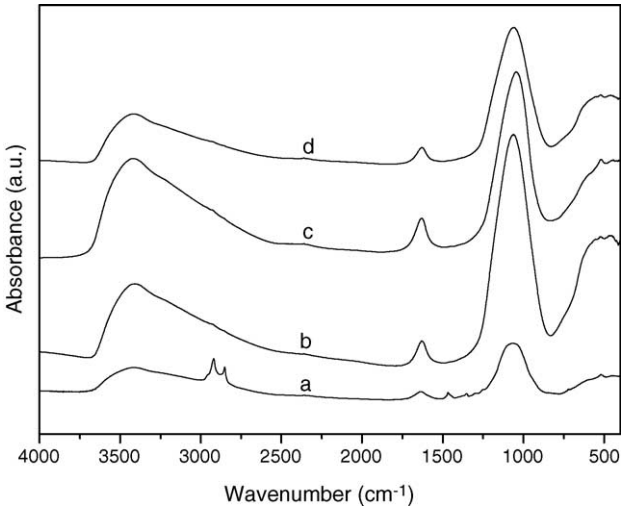

Fig. 8. Skeletal FT-IR spectra of the surfactant-synthesized—(a) ZrP-h and (b) ZrP-hc650 samples, and the surfactantless-synthesized—(c) ZrP-h and (d) ZrP-hc650 samples.

as Zr–O–P in the network of the samples, which is confirmed by the ^{31}P NMR.

Infrared spectroscopic characterization also reveals the presence of acid sites in these zirconium phosphate samples. Fig. 9 reports the in situ FT-IR spectra of the surfactant-synthesized ZrP-hc650 and ZrP-hc800 samples in the range of 4000–1200 cm^{-1} after evacuation at 200 and 450 °C over 3 h in a vacuum line, following the adsorption and desorption of ammonia molecules. The evacuated ZrP-hc650 samples exhibit two bands at 3771 and 3674 cm^{-1}, which are typical for isolated Zr–OH groups [34] and surface P–OH groups [35], respectively, and two weak bands at 1678 and 1460 cm^{-1}, which may be due to impurities of surface carbonate [34], besides the broad bands of the surface-adsorbed water and hydroxyl groups around 3500 and 1600 cm^{-1}, respectively. The bands at 3771 and 3674 cm^{-1} are still strong after evacuation at 450 °C (Fig. 9b), indicative of the persistence of large quantities of Zr–OH and P–OH groups in the present zirconium phosphate materials even after such a severe evacuation, though the quantity of surface hydroxyl groups decreases when the evacuation temperature elevated from 200 to 450 °C. The presence of the P–OH groups is normally indicative of the weak Brønsted acid sites. After in situ adsorption of NH_3, the bands of the Zr–OH and P–OH groups weaken obviously, even almost disappear. A new very broad band centered at 3200 cm^{-1}, stemming from the interaction of NH_3 with hydroxyl groups at 3771 and 3674 cm^{-1} which can be shifted toward lower wavenumber [36], appears. And another new large band around 1450 cm^{-1}, corresponding to the surface-adsorbed NH_4^+ groups, emerges (Fig. 9c). It is thus believed that the NH_3 molecules are indeed absorbed on the acid P–OH and Zr–OH groups. This suggests also that all the P–OH and Zr–OH groups are accessible to NH_3. The following desorption at 100 °C led to the emergence of the bands of 3770 and 3670 cm^{-1} again, and the weakening of the band of 1450 cm^{-1}. Further desorption at the elevated temperature of 300 °C results in almost recovery of the bands of Zr–OH and P–OH groups, and the decrease of the band intensity of 1450 cm^{-1} to be vague (Fig. 9e), indicating that the ammonia adsorption and desorption process is reversible. Indeed, significant quantities of the Zr–OH and P–OH groups and the surface hydroxyl groups can also be observed in the ZrP-hc800 sample after evacuation at 450 °C (Fig. 9f). The large number of surface hydroxyl groups is really significant to be used as active sites in catalysis or binding sites for surface modification in the multifunctionalization of the sample surface in order to extend the possible applications to advanced functional materials [33].

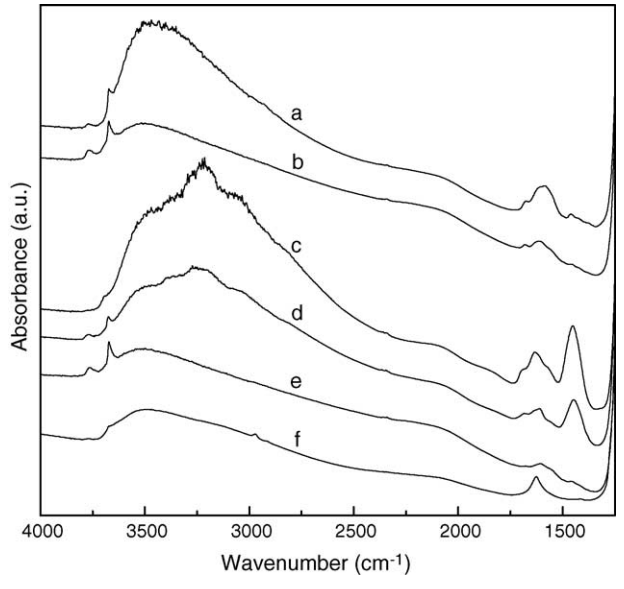

Fig. 9. In situ FT-IR spectra of the surfactant-synthesized ZrP-hc650 samples: (a) after evacuation at 200 °C for 3 h, (b) after evacuation at 450 °C for 3 h, and then (c) adsorption of NH_3 at room temperature for 15 min, (d) desorption at 100 °C for 15 min and (e) desorption at 300 °C for 15 min. (f) The spectrum of the surfactant-synthesized ZrP-hc800 sample after evacuation at 450 °C for 15 min.

For a porous material to be used in bulk-chemistry applications such as catalysis, in which reactant molecules need to readily access the interior pore structure but at the same time the internal surface area is maximized, a ramified pore structure with large pores leading to smaller and then smaller pores is desired (similar to the structure of lungs) [37]. Thus, hierarchical porous materials are indeed of great significance owing to their important role in the systematic study of structure–property relationship and their technological promise in applications [38]. Our synthesized zirconium phosphates possess not only the hierarchical macroporous structures with supermicroporous walls but also a large number of surface hydroxyl groups and acid sites. Such materials are really applicable as catalysts and catalyst supports, and accessible for the design of functional and structured one-pot reactors. It will be interesting to test

the catalytic performance of our materials in acid catalytic reaction.

4. Conclusions

Thermally stable macroporous zirconium phosphates with supermicroporous walls have been synthesized in the absence or presence of the surfactant Brij 56. The macropores are in a regular array with the diameters ranging from 300 to 800 nm, parallel to each other, and extend throughout almost the whole particles. The macroporous framework is amorphous and supermicroporous with a disordered wormhole-like assembly. Surprisingly, the presence of surfactant did not favor the formation of macroporous structures. ^{31}P NMR spectra revealed the stable coordination environment of phosphorus atoms in the synthesized hierarchical zirconium phosphate samples. FT-IR spectra also revealed the presence of Zr–O–P network and the presence of acid sites and surface hydroxyl groups in these catalyst materials. It is believed that, due to their attractive properties, such hierarchical materials should be significant and find numerous practical application potential in the fields of catalysis and materials science.

Acknowledgements

This work was supported by the European Program of InterReg III (Programme France-Wallonie-Flandre, FW-2.1.5) and realized in the frame of the Belgian Federal Government PAI-IUAP 01/5 project.

References

[1] T.Z. Ren, Z.Y. Yuan, B.L. Su, Chem. Phys. Lett. 388 (2004) 83–86.
[2] C.T. Kresge, M.E. Leonowicz, W.J. Roth, J.C. Vartuli, J.S. Beck, Nature 359 (1992) 710–712.
[3] D. Zhao, Q. Huo, J. Feng, B.F. Chmelka, G.D. Stucky, J. Am. Chem. Soc. 120 (1998) 6024–6036.
[4] D.M. Antonelli, Microporous Mesoporous Mater. 33 (1999) 209–214.
[5] Z.Y. Yuan, T.Z. Ren, B.L. Su, Adv. Mater. 15 (2003) 1462–1465.
[6] B.T. Holland, C.F. Blanford, T. Do, A. Stein, Chem. Mater. 11 (1999) 795–805.
[7] B. Lebeau, C.E. Fowler, S. Mann, C. Farcet, B. Charleux, C. Sanchez, J. Mater. Chem. 10 (2000) 2105–2108.
[8] S.A. Davis, S.I. Burkett, N.H. Mendelson, S. Mann, Nature 385 (1997) 420–423.
[9] B.T. Holland, L. Abrams, A. Stein, J. Am. Chem. Soc. 121 (1999) 4308.
[10] L. Huang, Z. Wang, J. Sun, L. Miao, Q. Li, Y. Yan, D. Zhao, J. Am. Chem. Soc. 122 (2000) 3530.
[11] D. Kuang, T. Brezesinski, B. Smarsly, J. Am. Chem. Soc. 126 (2004) 10534–10535.
[12] D. Zhao, P. Yang, B.F. Chmelka, G.D. Stucky, Chem. Mater. 11 (1999) 1174.
[13] K.J. Nakanishi, J. Porous Mater. 4 (1997) 67.
[14] J.L. Blin, A. Léonard, Z.Y. Yuan, L. Gigot, A. Vantomme, A.K. Cheetham, B.L. Su, Angew. Chem. Int. Ed. 42 (2003) 2872–2875.
[15] T.Z. Ren, Z.Y. Yuan, B.L. Su, Langmuir 20 (2004) 1531–1534.
[16] A. Léonard, J.L. Blin, B.L. Su, Chem. Commun. (2003) 2568–2569.
[17] Z.Y. Yuan, A. Vantomme, A. Léonard, B.L. Su, Chem. Commun. (2003) 1558–1559.
[18] W. Deng, M.W. Toepke, B.H. Shanks, Adv. Funct. Mater. 13 (2003) 61–65.
[19] A. Clearfield, U. Costantino, in: G. Alberti, T. Bein (Eds.), Comprehensive Supramolecular Chemistry, vol. 7, Elsevier, Amsterdam, 1996, pp. 107–150.
[20] J. Jiménez-Jiménez, P. Maireles-Torres, P. Olivera-Pastor, E. Rodríguez-Castellón, A. Jiménez-López, D.J. Jones, J. Rozière, Adv. Mater. 10 (1998) 812–815.
[21] Y. Sun, P. Afanasiev, M. Vrinat, G. Coudurier, J. Mater. Chem. 10 (2000) 2320–2324.
[22] U. Ciesla, S. Schat, G.D. Stucky, K.K. Unger, F. Schüth, Angew. Chem. Int. Ed. Engl. 35 (1996) 541.
[23] B. Tian, X. Liu, B. Tu, C. Yu, J. Fan, L. Wang, S. Xie, G.D. Stucky, D. Zhao, Nat. Mater. 2 (2003) 159–163.
[24] T.Z. Ren, Z.Y. Yuan, B.L. Su, Chem. Commun. (2004) 2730–2731.
[25] M. Kruk, M. Jaroniec, Chem. Mater. 13 (2001) 3169–3183.
[26] J.L. Blin, L. Gigot, A. Leonard, B.L. Su, Stud. Surf. Sci. Catal. 143 (2002) 1035.
[27] XPS Handbook of the Elements and Native Oxides, XPS International Inc., 1999, http://www.xpsdata.com/PDF/zr_no.pdf.
[28] S.J. Splinter, R. Rofagha, N.S. Mcintyre, U. Erb, Surf. Interface Anal. 24 (1996) 81.
[29] J.P. Chang, Y.S. Lin, J. Appl. Phys. 90 (2001) 2964–2969.
[30] M.S. Kim, Y.D. Ko, J.H. Hong, M.C. Jeong, J.M. Myoung, I. Yun, Appl. Surf. Sci. 227 (2004) 387–398.
[31] A. Sayari, I. Moudrakovski, J.S. Reddy, Chem. Mater. 8 (1996) 2080–2088.
[32] C. Schmutz, P. Barboux, F. Ribot, F. Taulelle, M. Verdaguer, C. Fernandez-Lorenzo, J. Non-Cryst. Solids 170 (1994) 250–262.
[33] T.Z. Ren, Z.Y. Yuan, B.L. Su, Chem. Phys. Lett. 374 (2003) 170–175.
[34] G.A.H. Mekhemer, Colloids Surf. A 141 (1998) 227–235.
[35] G. Busca, V. Lorenzelli, P. Galli, A. La Ginestra, P. Patrono, J. Chem. Soc., Faraday Trans. 183 (1987) 853.
[36] B.L. Su, D. Barthomeuf, J. Catal. 139 (1993) 81–92.
[37] T. Sen, G.J.T. Tiddy, J.L. Casci, M.W. Anderson, Angew. Chem. Int. Ed. 42 (2003) 4649–4653.
[38] B.L. Su, A. Léonard, Z.Y. Yuan, C. R. Chim. 8 (2005) 713–726.